Available online at www.sciencedirect.com
SCIENCE DIRECT®
Geochimica et Cosmochimica Acta 70 (2006) 1309–1321
Geochimica
www.elsevier.com/locate/gca

Comparative planetary mineralogy: Implications of martian and terrestrial jarosite. A crystal chemical perspective

J.J. Papike, J.M. Karner *, C.K. Shearer

Institute of Meteoritics, Department of Earth and Planetary Sciences, University of New Mexico, Albuquerque, NM 87131, USA

Received 6 July 2005; accepted in revised form 1 November 2005

Abstract

The importance of the discovery of jarosite at the Meridiani Planum region of Mars is discussed. Terrestrial studies demonstrate that jarosite requires a unique environment for its formation, crystallizing from highly acidic (pH < 4) S-rich brines under highly oxidizing conditions. A likely scenario for jarosite formation on Mars is that degassing of shallow magmas likely released SO_2 that reacted with aqueous solutions in shallow aquifers or on the martian surface. This interaction forms both H_2SO_4 and H_2S. A martian oxidant must be identified to both oxidize H_2S to produce the required acidity of the fluid, and to oxidize Fe^{2+} to Fe^{3+}. We suggest that reactions involving both sulfur and the reduction of CO_2 to CO may provide part of the answer. The jarosite crystal structure is truly remarkable in terms of its tolerance for the substitution of a large number of different cations with different ionic radii and charges. The structure accommodates hydrogen, oxygen, and sulfur, the stable isotope systematics of which are strong recorders of low-temperature fluid-rock-atmosphere interactions. Jarosite has been proven to be a robust chronometer for Ar–Ar and K–Ar dating techniques, and there is every reason to believe that U–Pb, Rb–Sr, and Nd–Sm techniques for older jarosite from Mars will also be robust. Although the discovery of jarosite on Mars alone, with no other analytical measurements on the phase, has given us insights to martian surficial processes, the true power of jarosite can not be exploited until jarosite is sampled and returned from Mars. Mars sample return is a long way off but, until then, we should be vigilant about examining martian meteorites for alteration assemblages that contain jarosite. A suite of jarosite samples representing a significant time span on Mars may hold the key to reading the record of martian atmospheric evolution.

1. Introduction

This is a paper in our comparative planetary mineralogy series where specific minerals that occur on different planetary bodies are compared and contrasted. We use this approach to take advantage of the natural laboratory conditions present on different planetary bodies (e.g., different oxygen fugacity, atmospheric pressure and composition, ambient temperature and temperature range, etc.). This approach has provided useful insights into differing planetary processes (e.g., Papike et al., 2005, and included references). Our previous studies in this series emphasized phases in planetary basalts such as pyroxene, olivine, plagioclase, and spinel. This paper is our first consideration of lower temperature minerals that crystallize from aqueous solutions (not melts) and specifically addresses the jarosite–alunite group of sulfates found on Earth and Mars. This study differs from our others in another way because past studies considered samples from different planetary bodies (Earth, Moon, Mars, 4 Vesta) but analyzed in terrestrial laboratories, where the full power of state of the art analytical instruments were used. This study refers to data collected in terrestrial laboratories for terrestrial jarosite–alunite. For martian jarosite we use data collected by the Mars Exploration Rover (MER) Mössbauer instrument (Klingelhöfer et al., 2004). The Mössbauer instrument has identified jarosite and hematite as important phases in outcrop and regolith of the equatorial site Meridiani Planum but could not provide the detailed chemistry

* Corresponding author.
E-mail address: jkarner@unm.edu (J.M. Karner).

0016-7037/$ - see front matter © 2005 Elsevier Inc. All rights reserved.
doi:10.1016/j.gca.2005.11.004

(major, minor, and trace), stable isotope data for sulfur, hydrogen, and oxygen, or ages from Ar–Ar or K–Ar techniques that terrestrial laboratories have provided for terrestrial samples. We will have to wait for martian sample return from surface deposits before similar measurements can be performed on martian sulfates.

The occurrence and potential of terrestrial jarosite is summarized by Lueth et al. (2005). Jarosite [$KFe_3(SO_4)_2(OH)_6$] mainly forms in highly acidic and oxidizing environments and is a relatively common mineral in the weathering zones of pyrite-bearing ore deposits (supergene jarosite). A second occurrence of the sulfate mineral is in near-surface playa sediments in acid-saline lakes, from aqueous sulfate derived either from the oxidation of pyrite and transported many kilometers by groundwater, or from sulfate aerosols transported from seawater (sedimentary jarosite). Jarosite also forms from the aqueous sulfate derived from the oxidation of H_2S in epithermal environments and hot springs commonly associated with volcanism (steam-heated jarosite).

This comparative planetary mineralogy study of martian and terrestrial jarosite is being undertaken because we would like to have a positive impact on future martian missions in terms of in situ instrumentation and potential sampling sites on the martian surface. The timing of this contribution was also inspired by the special issue of Chemical Geology (2005) volume 215 "Geochemistry of sulfate minerals in high- and low-temperature environments: a Tribute to Robert O. Rye". This series of papers is an outstanding testimonial to the power of sulfate minerals as recorders of terrestrial rock/fluid interactions. Another treasure trove of information on sulfate minerals is provided in "Sulfate Minerals" (Alpers et al., 2000), Reviews in Mineralogy and Geochemistry, Vol. 40.

In the following we discuss the crystal chemistry of jarosite and the occurrence and potential genesis of jarosite on Mars. Next, we will assess studies of terrestrial jarosite–alunite occurrences where state-of-the-art analytical techniques were used for obtaining chemistry, stable isotope geochemistry, and radiogenic isotopic ages. This summary of terrestrial occurrences should make it abundantly clear why we must return Mars surface samples and why the Meridiani Planum location should be a serious contender for the landing location for one of the Mars Science Laboratory (MSL) rovers. Lastly, we will consider ways that future approved space flight in situ instrumentation (e.g., the chemical and mineralogic analyzer, CheMin, (Vaniman et al., 1998; Sarrazin et al., 2000), a combined X-ray diffraction (XRD)/X-ray fluorescence (XRF) instrument for the MSL mission) will contribute to our characterization and interpretation of jarosite on Mars.

2. Crystal chemistry

Although there are more than 40 mineral species with the fundamental alunite crystal structure (Stoffregen et al., 2000), this review will emphasize alunite, $KAl_3(SO_4)_2(OH)_6$; natroalunite, $NaAl_3(SO_4)_2(OH)_6$; jarosite, $KFe_3^{3+}(SO_4)_2(OH)_6$; and natrojarosite, $NaFe_3^{3+}(SO_4)_2(OH)_6$. We use the general formula $AB_3(XO_4)_2(OH)_6$ (Scott, 1987) where A is a 12-fold coordinated site that can contain monovalent cations K, Na, Rb, etc., divalent cations Ca, Pb, Ba, Sr, etc., and trivalent cations, REE, etc. The B position represents an octahedral site that usually contains trivalent Fe and Al but can also include Pb^{2+}, Zn^{2+}, Mg^{2+}, etc. The X position represents the tetrahedral site and contains S, P, As, Sb, etc. In this discussion, for the purpose of simplicity, we consider only structures with S^{6+} or P^{5+} in the tetrahedral site; 6 (OH) groups, Fe^{3+}, Al, and Mg in the octahedral B-site; and K, Na, Rb, Ca^{2+}, Pb^{2+}, Sr^{2+}, Ba^{2+}, Eu^{2+}, the trivalent REEs, Nd, and Sm and vacancies in the 12-coordinated A-site.

Our discussion of the crystal structure is derived from Menchetti and Sabelli (1976) and Okada et al. (1982). Alunite and jarosite crystallize in space group $R\bar{3}m$, with $Z = 3$. For alunite there are 3 K, 9 Al, 18 (OH) groups, 24 oxygens, and 6 sulfur atoms per unit cell. The unit cell parameters are alunite, $a = 7.020$ Å, $c = 17.223$ Å; Na–alunite, $a = 7.010$ Å, $c = 16.748$ Å; jarosite, $a = 7.315$ Å, $c = 17.224$ Å; Na–jarosite, $a = 7.327$ Å, $c = 16.634$ Å (Menchetti and Sabelli, 1976). The *a*-axis increases with the substitution of Fe^{3+} for Al in the octahedral site, and the *c*-axis decreases with the substitution of Na for K in the 12-coordinated site. Thus, these unit cell variations can be used for estimating the Na/K and Al/Fe^{3+} ratio in solid solution among the end-members alunite–natroalunite–jarosite–natrojarosite. This will be a very important application of the XRD on the Mars CheMin instrument (discussed subsequently).

The jarosite–alunite crystal structure is beautiful in its simplicity and is truly remarkable (Figs. 1 and 2) in that it can accommodate many elements in the periodic table. Fig. 1A shows the jarosite structure projected down the *c*-axis. Fig. 1B illustrates selected symmetry elements in space group $R\bar{3}m$ including three fold axes (3-fold, $\bar{3}$ axis = 120° rotation plus an inversion; and 3-fold screw axis = 120° rotation plus translation along *c*), and mirror planes parallel to *c* (solid lines). Symmetry elements perpendicular to the *c*-axis are not shown nor are the glide planes. Table 1 illustrates which type of crystallographic site (general or special) each atom is located in. If an atom is located in a unit cell with no special relation to any of the symmetry elements it is said to be located in a general position. Such atoms have the maximum number of repeat operations in the crystal unit cell (multiplicity). In space group $R\bar{3}m$, an atom in a general position is repeated 36 times. No atoms in the jarosite structure occupy a general position. All occupy special positions with various degrees of specialty. The more specialized the lower the multiplicity. For example, the K atom (purple sphere) sits on a $\bar{3}$ axis at the corner of the unit cell and has multiplicity 3, or 3 K atoms per unit cell. The K atom sits in a 12-coordinated site and is coordinated by 6 oxygen ligands and

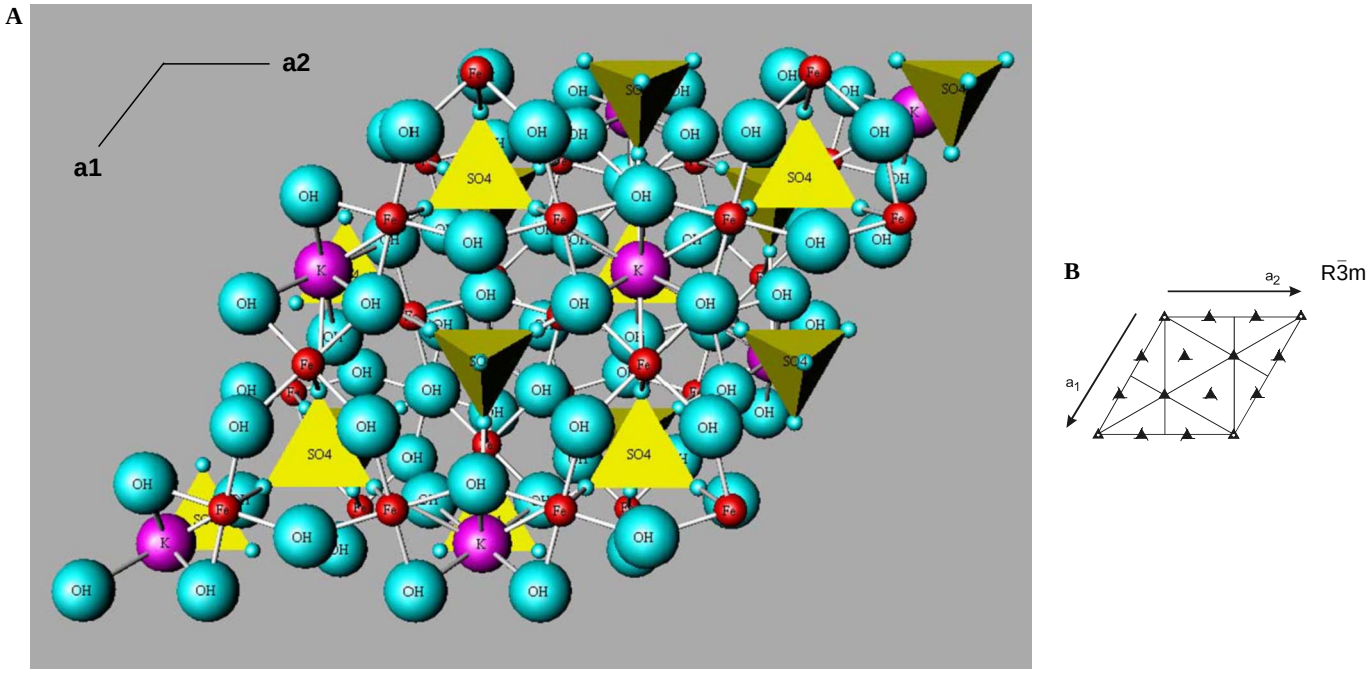

Fig. 1. (A) The crystal structure of jarosite projected down the *c*-axis. Diagram compliments of Eric Dowty. See text for discussion. (B) Space group projection down the *c*-axis showing only some of the symmetry elements. See text for discussion.

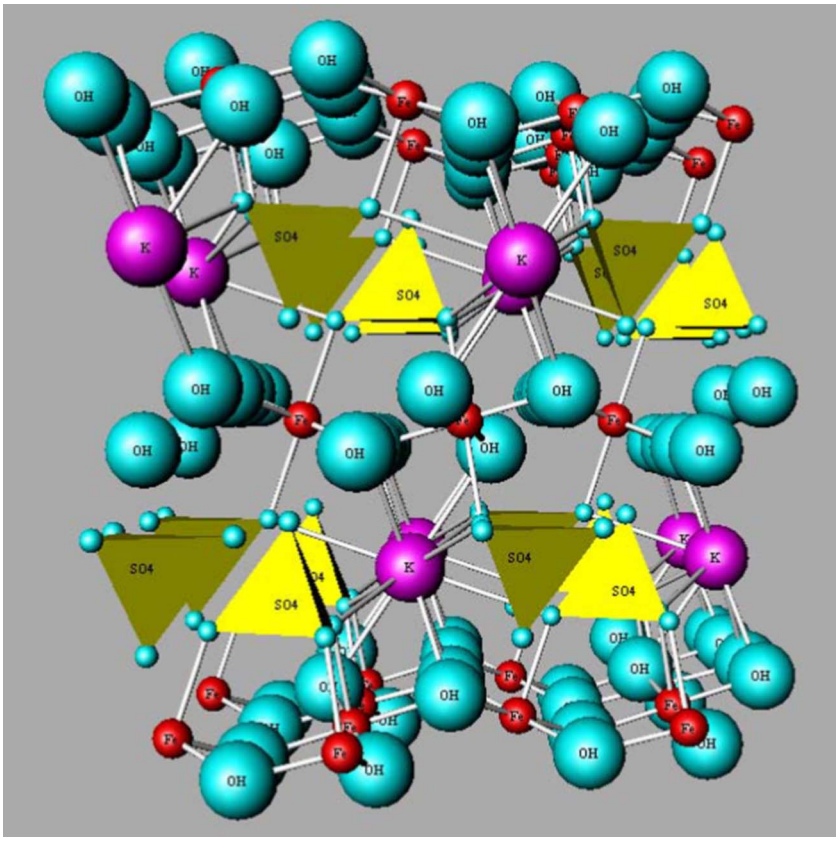

Fig. 2. The crystal structure of jarosite projected down the *a*-axis. Diagram compliments of Eric Dowty. See text for discussion.

6 OH ligands. All 6 oxygen ligands are symmetrically identical and all 6 OH groups are symmetrically identical. This is because of the $\bar{3}$ operation, which rotates each ligand 3 times by 120° rotations and inverts all three through the position of the K atom to 3 more positions. Thus the A-site has a highly symmetrical coordination with 6 identical

Table 1
Crystal structure aspects of alunite and jarosite: Z, number of formula units per unit cell = 3

Atom, group	Wyckoff site Notation	Site symmetry	Multiplicity	
K	a	$\bar{3}$m	3	
Fe^{3+}, Al	d	2/m	9	
(OH)	h	m	18	
O (1)	c	3m	6	= 24
O (2)	h	m	18	
S	c	3m	6	

Jarosite $KFe_3^{3+}(SO_4)_2(OH)_6$. Natrojarosite $NaFe_3^{3+}(SO_4)_2(OH)_6$. Alunite $KAl_3(SO_4)_2(OH)_6$. Natroalunite $NaAl_3(SO_4)_3(OH)_6$. Atoms and OH groups per unit cell: 3 K; 9 (Fe^{3+}, Al); 18 (OH) groups; 24 O^{2-}; 6 S.

Table 2
Selected interatomic distances for alunite and jarosite (Menchetti and Sabelli, 1976)

Alunite		Jarosite	
S–O (1)	1.458 Å × 1	S–O (1)	1.465 Å × 1
S–O (2)	1.489 Å × 3	S–O (2)	1.481 Å × 3
K–O (2)	2.836 Å × 6	K–O (2)	2.978 Å × 6
K–(OH)	2.866 Å × 6	K–(OH)	2.828 Å × 6
Al–O (2)	1.947 Å × 2	Fe^{3+}–O (2)	2.058 Å × 2
Al–(OH)	1.879 Å × 4	Fe^{3+}–(OH)	1.975 Å × 4

K–OH bonds and 6 identical K–O bonds (Table 2). The Fe^{3+} atoms (red spheres) occupy a site that sits on a 2-fold axis with a mirror perpendicular to it. It is coordinated by 4 symmetrically identical OH groups and 2 symmetrically identical oxygen atoms. Thus, there are 4 identical Fe^{3+}–O distances and 2 Fe^{3+}–O distances (Table 2). The sulfur atoms occupy a site that sits on a 3-fold rotation axis and this site has multiplicity 6 or 6 sulfur atoms per unit cell. All sulfur atoms (yellow tetrahedra with sulfur at the center) are in symmetrically and energetically equivalent positions. One of the oxygen ligands (O1) coordinating sulfur sits on the same 3-fold axis that the sulfur atom sits on and thus provides one S–O(1) bond length (Table 2). The other oxygen O(2) that coordinates S is off the 3-fold axis and thus is repeated three times by the 3-fold operation. This provides three identical S–O(2) bond lengths (Table 2). Thus all three types of crystallographic sites, A, B, and X are highly symmetrical. When the jarosite crystal structure is projected down the *a*-axis (Fig. 2) we see additional features, which show that the jarosite structure can be described as having alternating layers of Fe^{3+} octahedra, and layers composed of sulfur tetrahedral and K sites.

Now we look at the possible chemical substitutions in the jarosite–alunite structure for the specific elements mentioned above. Note Fig. 3 for a diagram that shows specific crystallographic site substitutions. We use the techniques that Papike has used in the past for amphibole, pyroxene, and olivine (e.g., Papike et al., 2005). These involve a chemical reference quadrilateral (QUAD), and in this case has end-members alunite–natroalunite–jarosite–natrojarosite (Fig. 4). Any chemical component that substitutes for a QUAD cation, and has a charge different from that QUAD cation (monovalent in A-site; trivalent in B-site, and hexavalent in the X-site), is referred to be in the OTHERS group. Because minerals require charge neutrality, coupled-substitutions are involved. Note Table 3 for some examples. For example, if Ba^{2+} substitutes for K in the A-site a charge excess of +1 is involved and requires a charge deficiency of −1 to provide charge neutrality. A few examples of charge balanced coupled-substitutions with Ba are: Ba (A-site) coupled with a vacancy (A-site); Ba (A-site) coupled with P^{5+} (X-site); Ba (A-site) coupled with Mg (B-site).

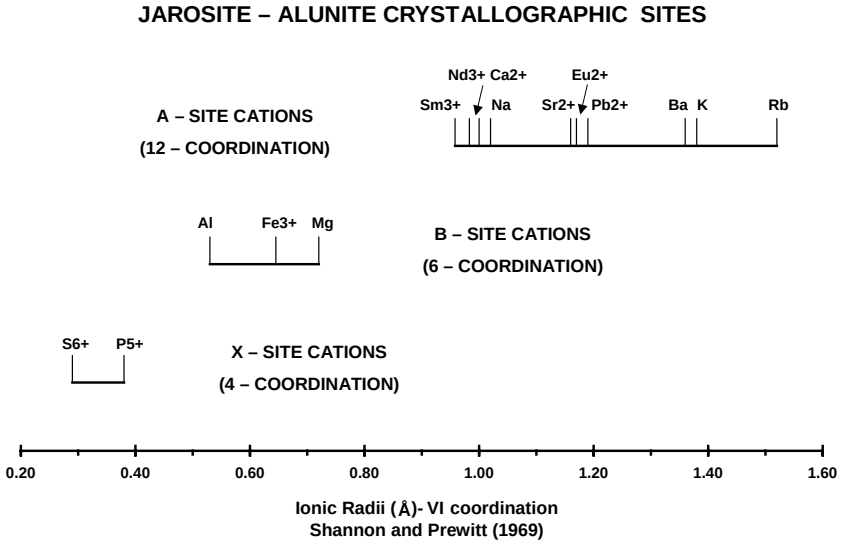

Fig. 3. Diagram illustrating crystallographic site substitutions in jarosite–alunite for a select set of cations. The 12-coordinated A-site accommodates a large range of ionic radii for monovalent, divalent, and trivalent cations. We assume the octahedral B-site contains Al, Fe^{3+}, and Mg, and that the tetrahedral X-site accommodates S^{6+} and P^{5+}.

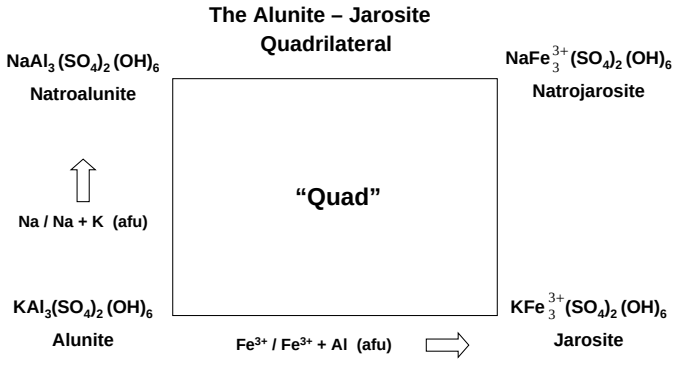

Fig. 4. The alunite–jarosite quadrilateral. See text for discussion.

Table 3
Charge balance excess and deficiencies substitutions (OTHERS) relative to the jarosite–alunite (QUAD)

Excess	Deficiency
${}^{A}R^{2+}$ = (Ca^{2+}, Pb^{2+}, Sr^{2+}, Ba^{2+}, Eu^{2+})	${}^{B}Mg^{2+}$
${}^{A}2R^{3+}$(= Nd^{3+}, Sm^{3+})	${}^{X}P^{5+}$
	${}^{A}\square$ (= vacancy)
Some possible coupled substitutions	
${}^{A}R^{2+}$–${}^{A}\square$	
${}^{A}R^{2+}$–${}^{X}P^{5+}$	
${}^{A}R^{2+}$–${}^{B}Mg^{2+}$	
${}^{A}R^{3+}$–$2{}^{A}\square$	
${}^{A}R^{3+}$–$2{}^{B}Mg^{2+}$	
${}^{A}R^{3+}$–$2{}^{X}P^{5+}$	
${}^{A}R^{3+}$–(${}^{B}Mg^{2+}$ + ${}^{X}P^{5+}$)	
${}^{A}R^{3+}$–(${}^{A}\square$ + ${}^{X}P^{5+}$)	
${}^{A}R^{3+}$–(${}^{A}\square$ + ${}^{B}Mg^{2+}$)	

The bond energies for each cation in each site determines the partitioning behavior of the cations between the jarosite structure and the aqueous fluid from which it precipitated. Thus, if we know the partition coefficient (*D*s) for each cation (mineral/fluid) we can calculate the concentration of the cation in the coexisting fluid if we know the concentration in the jarosite crystal. We can also obtain the same information if we find fluid inclusions. Likewise the systematics of the stable isotope partitioning of sulfur and oxygen between jarosite and fluid depends on how many distinct sites (and distinct bonds within a site) are involved and the associated bond strengths. Also, the jarosite–alunite structure enables the use of several types of radiogenic geochonometers including U–Pb, Rb–Sr, K–Ar, Ar–Ar, and Sm–Nd. This is because all parent and daughter isotopes are nicely accommodated in the 12-coordinated A-site. Of course the viability of each of these chronometers depends on how old the jarosite is (different half-lives for different systems) and whether the isotopes have been reset by any process since crystallization. By now the reader should see the potential of jarosite–alunite as a recorder of low-temperature surficial process on the martian surface. Examples of this use of jarosite for both martian and terrestrial occurrences are documented below.

3. Models for terrestrial jarosite formation and the stable isotope systematics used to determine them

In this section we define three models for jarosite formation on Earth and discuss how these environments can be distinguished from one another using stable isotope systematics. The stable isotope systematics we are interested in are $\delta^{34}S$, δD, $\delta^{18}O_{OH}$, and $\delta^{18}O_{SO_4}$ in jarosite; we will not discuss stable isotopes systematics for alunite. Neither will we discuss hydrothermal environments that produce alunite and not jarosite, but these are reviewed thoroughly by Rye (2005).

Fig. 5 illustrates the supergene and steam-heated environments in which jarosite can form (after Rye, 2005; Hurowitz et al., 2005). Both SO_2 and H_2S exsolve from late crystallizing magma, and oxidation of either of these species is a requisite to generate the acidic fluids needed to form jarosite. Two oxidation steps are required to process SO_2: (1) an H_2O plus SO_2 reaction that produces H_2S and H_2SO_4 and (2) oxidation of H_2S to provide the low pH required for jarosite stability. Processing of exsolved H_2S only involves the latter oxidation step (note reactions in Fig. 5). On Earth, atmospheric oxygen provides for the oxidation of H_2S to H_2SO_4 and Fe^{2+} to Fe^{3+}. The oxidation of pyrite leads to supergene jarosite, while the oxidation of H_2S leads to steam-heated jarosite. Both oxidation of pyrite and H_2S take place in the vadose zone where rocks can not buffer the pH. On Mars, atmospheric CO_2 reduction to CO is a possible oxidation mechanism. The third occurrence of terrestrial jarosite is sedimentary (not illustrated). Sedimentary jarosite forms in the near-surface sediments of acid-saline lakes, possibly from wind-blown sulfate aerosols derived from nearby seawaters (Alpers et al., 1992).

Jarosite contains both sulfate (SO_4) and hydroxyl (OH) sites and thus the $\Delta^{18}O_{SO_4\text{-}OH}$ can be used as a single-mineral geothermometer. This thermometer is only valid if the SO_4 attained equilibrium with the water in the hydrothermal fluid, and retrograde exchange did not occur at the OH site during the final stages of mineralization (Rye and Stoffregen, 1995). The jarosite SO_4 and OH components are separated for $\delta^{18}O$ analysis by chemical extraction, which is discussed in Lueth et al. (2005). An application of this geothermometer is shown in Fig. 6, where $\delta^{34}S$ values are plotted against $\delta^{18}O$ values for jarosite from the Rio Grande Rift (RGR) deposits of southern New Mexico and northern Mexico (after Lueth et al., 2005). Tie lines connect $\delta^{18}O_{SO_4}$ and $\delta^{18}O_{OH}$ values of the same sample. The $\Delta^{18}O_{SO_4\text{-}OH}$ of most of the jarosite samples ranges from 9.3‰ to 13‰. This range can then be used to determine the temperature of formation on the basis of the experimental fractionations of Rye and Stoffregen (1995), as are shown in Eq. (1).

$$10^3 \ln \alpha_{\text{jarosite}(SO_4\text{-}OH)} = 1.43(10^6/T^2) + 1.86. \quad (1)$$

The fractionation factor α is equal to the $^{18}O/^{16}O$ ratio of the sulfate over the hydroxyl, and is commonly expressed

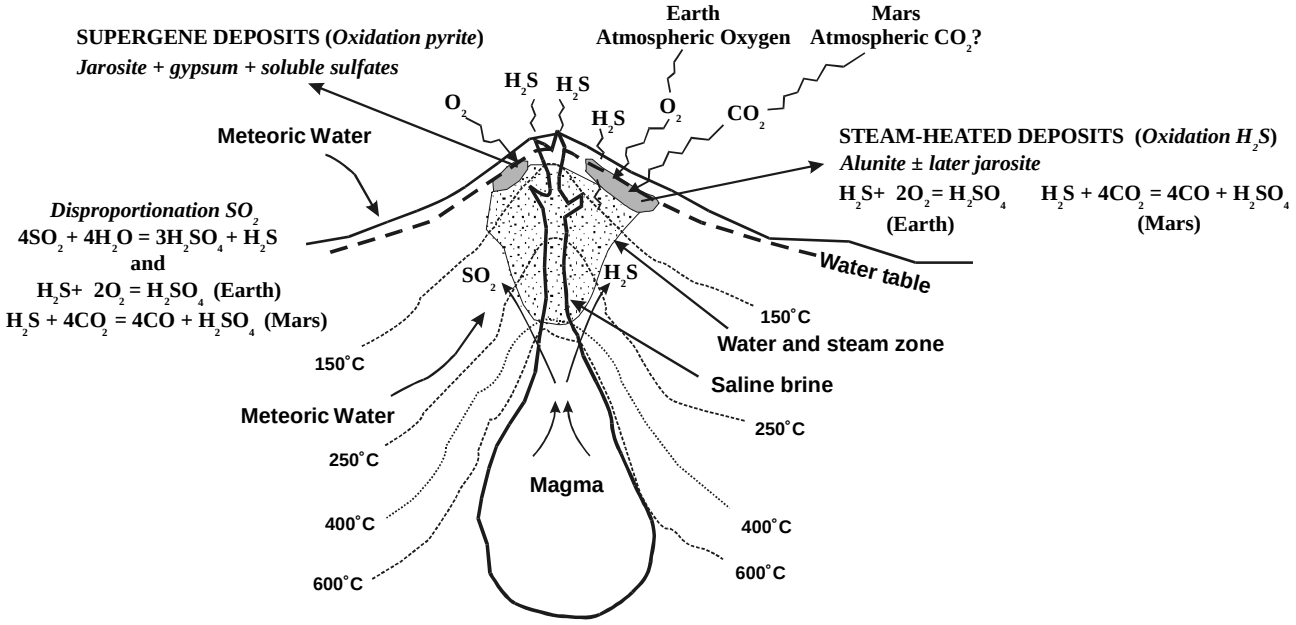

Fig. 5. Schematic diagram illustrating the supergene and steam-heated terrestrial environments in which jarosite can form (after Rye, 2005; Hurowitz et al., 2005). Both SO_2 and H_2S exsolve from late crystallizing magma. Two oxidation steps are required to process SO_2: (1) an H_2O plus SO_2 reaction that produces H_2S and H_2SO_4 and (2) oxidation of H_2S to provide the low pH required for jarosite stability. On Earth, atmospheric oxygen provides for the oxidation of H_2S to H_2SO_4 and Fe^{2+} to Fe^{3+}. The oxidation of pyrite or H_2S takes place in the vadose zone where rocks can not buffer the pH. On Mars, atmospheric CO_2 reduction to CO is a possible oxidation mechanism. Note in simplifying this diagram from Rye (2005) we did not illustrate environments that produce alunite but not jarosite. See text for further discussion.

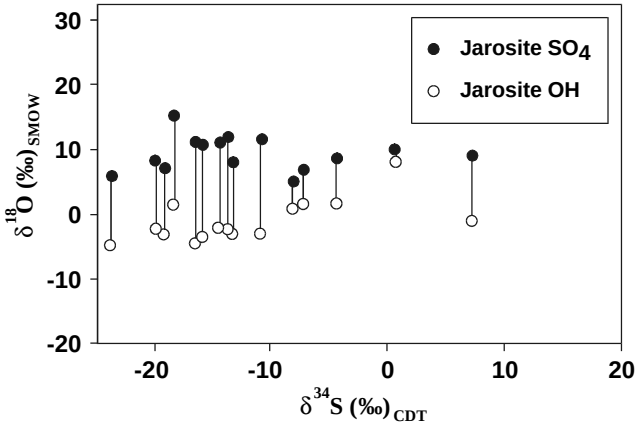

Fig. 6. Diagram showing $\delta^{34}S$ versus $\delta^{18}O$ for jarosite from the Rio Grande Rift (RGR) deposits of southern New Mexico and northern Mexico (after Lueth et al., 2005). Tie lines connect $\delta^{18}O_{SO_4}$ and $\delta^{18}O_{OH}$ values of the same sample. The jarosite sulfate (SO_4) and hydroxyl (OH) components are separated for $\delta^{18}O$ analysis by chemical extraction, discussed in Lueth et al. (2005). The $\Delta^{18}O_{SO_4\text{-}OH}$ can be used to determine temperature of formation on the basis of the experimental fractionations of Rye and Stoffregen (1995). The calculated temperatures for this data give a range between 240 and 80 °C. See text for discussion.

as $10^3 \ln \alpha$ because this expression is a very close approximation to the permil fractionation. Inserting the data into Eq. (1) gives a range of temperatures between 240 and 80 °C, which is consistent with the range of filling temperatures of fluid inclusions in late fluorites, and a single jarosite sample in RGR deposits (Lueth et al., 2005). The temperature of RGR jarosite formation, its occurrence in the field, and the absence of pyrite for oxidation, requires a hydrothermal origin in a steam-heated environment, where acidic conditions were achieved by the oxidation of H_2S derived from deep hydrothermal fluids.

The $\delta^{34}S$ values of jarosite from four different terrestrial locations are shown in Fig. 7. Australian lakes data are from acid-hypersaline lake deposits (Alpers et al., 1992), and are classified as sedimentary jarosite; Cascades data are from deposits in active andesite stratavolcanoes (Zimbelman et al., 2005), and are categorized as supergene jarosite; Crofoot-Lewis data are from hot spring deposits in northwestern Nevada (Ebert and Rye, 1997), and are noted as steam-heated jarosite; and the RGR deposits are steam-heated and are illustrated in Fig. 6 and discussed in the preceding paragraph. The $\delta^{34}S$ values can be used to determine the source of sulfate in jarosite and the possible environment of deposition. For example, low $\delta^{34}S$ values for jarosite from the Cascades, Crofoot-Lewis, and RGR samples indicate sulfate was derived by either oxidation of H_2S or pyrite. This oxidation can take place in either a steam-heated or supergene environment. The high $\delta^{34}S$ values for the Australian lakes jarosite indicate sulfate was probably not derived from the oxidation of pyrite or H_2S. Instead, the authors (Alpers et al., 1992) point out that the $\delta^{34}S$ values for modern marine evaporites (21.5‰) and modern seawater (20‰) are very similar to the jarosite values (22‰). This suggests that the sulfate in the jarosite was derived from seawater, and that a likely mechanism of incorporation into internally draining basins of southern Australia is as wind-blown aerosols. Fig. 7 also

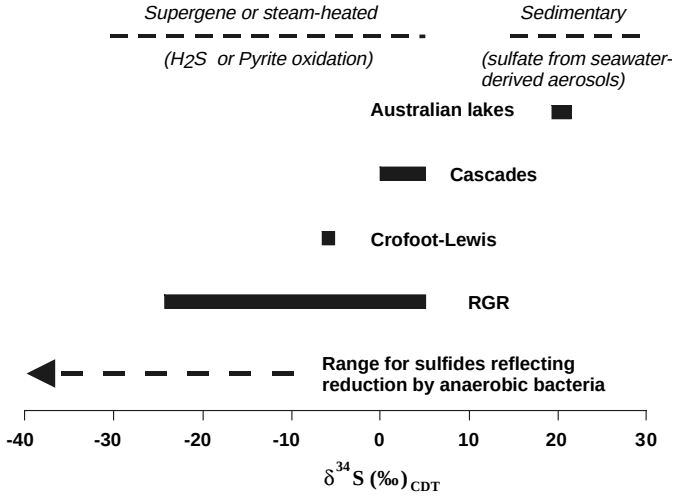

Fig. 7. $\delta^{34}S$ values of jarosite from four different terrestrial locations. Australian lakes data are from acid-hypersaline lake deposits (Alpers et al., 1992), and are classified as sedimentary jarosite; Cascades data are from deposits in active andesite stratavolcanoes (Zimbelman et al., 2005), and are categorized as supergene jarosite; Crofoot-Lewis data are from hot spring deposits in northwestern Nevada (Ebert and Rye, 1997), and are noted as steam-heated jarosite; and Rio Grande Rift (RGR) deposits are from mining districts in southern New Mexico and northern Mexico (after Lueth et al., 2005), and are classified as steam-heated jarosite. The $\delta^{34}S$ values can be used to determine the source of sulfate in jarosite and the possible environment of deposition. For example, low $\delta^{34}S$ values ($\sim -25‰$ to $5‰$) indicate sulfate was derived by either oxidation of H_2S or pyrite. This oxidation can take place in a steam-heated or supergene environment. High $\delta^{34}S$ values ($\sim 22‰$) for the Australian lakes jarosite indicate sulfate was most likely derived from seawater as wind-blown aerosols. Also shown is the $\delta^{34}S$ range for sulfides that have been reduced by anaerobic bacteria (Shearer et al., 1996). Diagram after Rye (2005).

shows the $\delta^{34}S$ range for sulfides that have been reduced by anaerobic bacteria (Shearer et al., 1996). Sulfides derived by reducing bacteria have very low $\delta^{34}S$ values down to $-40‰$; and thus hypothetical very low $\delta^{34}S$ values could suggest some bacterial action.

Figs. 8A and B are a summary of δD and $\delta^{34}S$ values versus $\delta^{18}O_{SO_4}$ values of jarosite from the same four locations as in Fig. 7 (see that figure caption for explanation of abbreviations). In Fig. 8A, the supergene jarosite sulfate field (SJSF), enclosed by the dashed line, delineates the range of values expected for supergene jarosite and is shown for reference (Rye and Alpers, 1997). The Crofoot-Lewis and Australian lakes plot out of the SJSF as should be expected, as these are steam-heated and sedimentary jarosite deposits, respectively. The Cascades (supergene jarosite) and RGR (steam-heated) lie approximately half in and half out of the SJSF and suggest that supergene and steam-heated jarosite produce similar δD and $\delta^{18}O_{SO_4}$ systematics. Also noted in Fig. 8A is the meteoric water line (MWL), which can be used along with the δD and $\delta^{18}O_{SO_4}$ systematics to determine the source of water in these environments. For example, the very low $\delta^{18}O_{SO_4}$ for Cascades jarosite indicate the oxygen in the sulfate was derived from isotopically light meteoric water, which is consistent with the presence of abundant snow and ice on volcano summits. Furthermore,

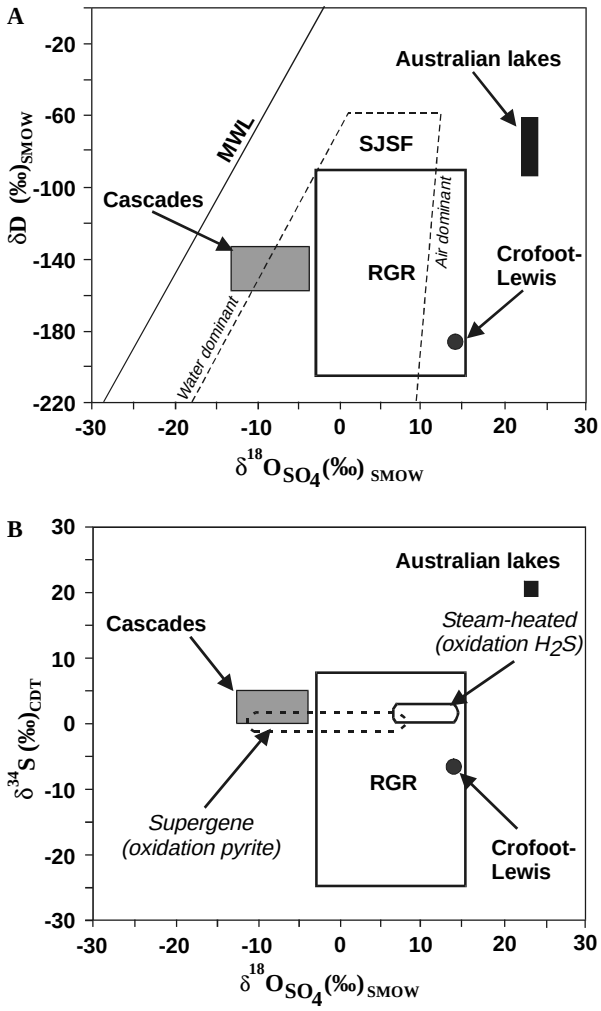

Fig. 8. (A) Summary of δD versus $\delta^{18}O_{SO_4}$ values of jarosite from the same four locations as in Fig. 7, see that figure caption for explanation of abbreviations. The Supergene jarosite sulfate field (SJSF), enclosed by the dashed line, delineates the range of values expected for supergene jarosite (Rye and Alpers, 1997). The meteoric water line (MWL) is also shown. See text for discussion. Diagram after Rye (2005). (B) Summary of $\delta^{34}S$ versus $\delta^{18}O_{SO_4}$ values of jarosite from the same as above. The fields for supergene and steam-heated deposits (Rye, 2005) are shown as ovals in dashed and solid lines. See text for discussion.

the data for jarosite in Fig. 8A can used to calculate the corresponding isotopic compositions of the parent fluids from which jarosite formed. Lueth et al. (2005) did this for the RGR deposits and found that jarosite parental fluids have calculated isotopic signatures (δD and $\delta^{18}O_{SO_4}$) similar to those of modern geothermal waters and meteoric waters in the present day rift.

Fig. 8B illustrates the $\delta^{34}S$ versus $\delta^{18}O_{SO_4}$ values of jarosite from the same four terrestrial environments, and serves to further define the origin of these jarosites. The fields for supergene and steam-heated deposits (Rye, 2005) are shown as ovals in dashed and solid lines. Here again we see that the Australian lakes data plots well out of the fields for supergene or steam-heated jarosite, as is expected for sedimentary jarosite. The Crofoot-Lewis data plots near

the steam-heated field, as expected, while the Cascade data overlaps the supergene field, also as expected. The RGR data plots again in both the supergene and steam-heated field, but here totally encompasses the steam-heated field, confirming these do indeed have a steam-heated origin.

4. Discussion

4.1. Martian jarosite

Kargel (2004) provides an introduction to the exciting early results of NASA's Opportunity rover which landed on Mars' Meridiani Planum, a smooth flat plain unlike any feature studied by earlier landers. Opportunity is the first Mars vehicle to sample bedrock, and these rocks consist of layers of iron oxides and hydrated Mg-, Ca-, and Fe-sulfates. The sediments that make up the layered rocks were deposited in, or altered by, acidic brines, and may be aeolian, volcanogenic, or chemical, but also have a significant basaltic component. The mineral jarosite, detected at Meridiani Planum, requires highly acidic conditions, which may explain the absence of calcite here, because calcium carbonate reacts to gypsum in acid sulfate solution. High sulfur to chlorine ratios and high iron contents suggest a temperature >265 K. The mineral assemblages and chemistry are similar to terrestrial acid mine drainage deposits. A more recent interpretation of these deposits is provided by McLennan et al. (2005).

Klingelhöfer et al. (2004) positively identified jarosite using the Mössbauer spectrometer on Opportunity. This study identified four major mineralogical components at Eagle Crater, jarosite- and hematite-rich outcrop, hematite-rich regolith, olivine-bearing regolith, and a pyroxene-bearing basaltic rock (Bounce rock). One sample found that jarosite made up 36% and hematite 37% of the Fe-containing minerals that could be studied by Mössbauer techniques.

Elwood Madden et al. (2004) report on jarosite as an indicator of water-limited chemical weathering on Mars. The authors point out that terrestrial jarosite persists over geologically relevant periods of time in arid environments but rapidly decomposes to produce oxyhydroxides in more humid climates. Elwood Madden et al. (2004) present equilibrium thermodynamic reaction-path simulations that constrain the range of possible conditions under which jarosite-containing assemblages are likely to have formed on Mars. They conclude that the presence of jarosite combined with residual basalt at Meridiani Planum indicates the alteration process did not proceed to completion, and following jarosite formation, arid conditions must have prevailed. They also conclude that continued water loss from the martian atmosphere gradually reduced the relative humidity to levels where hydrous phases exposed to the atmosphere could dehydrate producing hematite and anhydrite from iron hydroxides and gypsum (Fig. 9). In Fig. 9, the arrow starting at the upper left shows the reaction path followed during

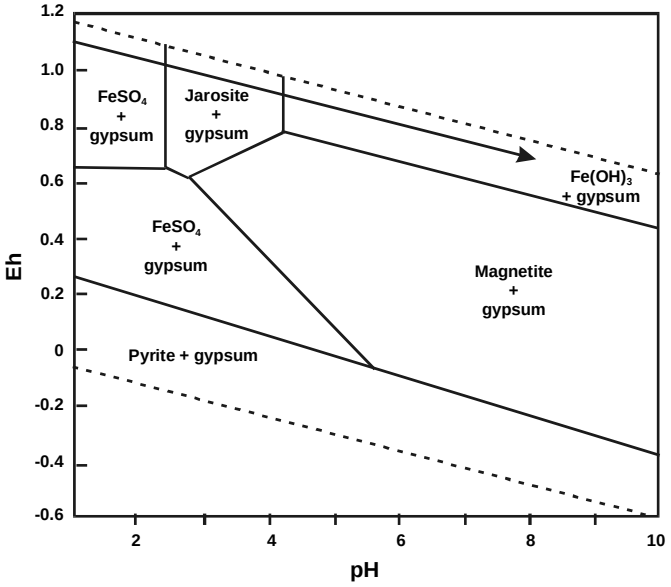

Fig. 9. Eh-pH diagram showing martian jarosite stability at 298 K. Diagram after Elwood Madden et al. (2004). See that paper for assumptions concerning diagram construction.

weathering of basalt by sulfate-bearing aqueous solutions buffered by the present martian atmosphere. Therefore, the observation of jarosite suggests a short-lived period of water-limited aqueous alteration.

Robert Rye (2005, personnel communication) provides an interpretation of the significance of martian jarosite:

> Jarosite requires a very unique environment for its formation. In the case of Mars there would have to be either (or both) pyrite in the rocks or H_2S in hydrothermal fluids that oxidized. That oxidation had to take place in the "vadose" zone, where the rocks could not buffer the pH of the jarosite parent fluids. The most likely scenario is that sulfur gases were released from shallow magmas, largely as SO_2, and then underwent disproportionation on condensation in water below 400 °C to produce SO_4^{2-} and H_2S. Near-surface H_2S was then oxidized to produce the low pH fluids that precipitated jarosite.

The challenge for these models and the Mars exploration program is to identify the martian oxidant responsible for the oxidation of iron from Fe^{2+} to Fe^{3+}. The following reactions might be involved:

STEP 1 (oxidation–reduction reaction, 6 electrons transferred)

$$2SO_2 + 2H_2O + 4Fe^{2+} = H_2S + SO_4^{2-} + 4Fe^{3+} + 2(OH)^-$$

STEP 2 (oxidation of H_2S, reduction of carbon, 8 electrons transferred)

$$4CO_2 + H_2S = 4CO + H_2SO_4$$

STEP 3 (precipitation of jarosite from low-pH brines)

$$K^+ + 2SO_4^{2-} + 6(OH)^- + 3Fe^{3+} = KFe_3(SO_4)_2(OH)_6(\text{jarosite})$$

4.2. Case study: hydrothermal jarosite in acid-sulfate mineralization, southern Rio Grande Rift, New Mexico— Mexico

Lueth et al. (2005) provides a study demonstrating the power of jarosite as a recorder of near-surface fluid-rock processes on Earth. Approximately 29 mining districts along the Rio Grande Rift in southern New Mexico contain deposits containing fluorite–barite–jarosite and additional deposits occur south of the Basin and Range province near Chihuahua, Mexico. Jarosite occurs in many of these deposits as a late-stage hydrothermal mineral precipitating with fluorite or in veinlets that crosscut barite. In these deposits jarosite is followed by natrojarosite. These deposits range in age from 10 to 0.4 Ma on the basis of Ar–Ar dating of jarosite. As discussed above, most oxygen isotope data indicate that jarosite precipitated between 80 and 240 °C, which is consistent with the range of filling temperatures of fluid inclusions in fluorite throughout the rift and in jarosite from Peña Blanca, Chihuahua, Mexico (180 °C). Thus, these jarosites have a hydrothermal origin in a shallow steam-heated environment wherein the low-pH necessary for the precipitation of jarosite was achieved by the oxidation of H_2S derived from deeper hydrothermal fluids. The requisite H_2SO_4 for jarosite formation was derived from the oxidation of H_2S. Jarosite formed at shallow levels after the pH buffering capacity of the host rock (typically limestone) was neutralized by precipitation of earlier minerals. These jarosites record episodic hydrologic processes that operated in the rift over the last 10 million years.

Fig. 10 represents the stability field of jarosite at 200 °C and 100 bars that represent the conditions represented for this study. See Lueth et al. (2005) for compositional assumptions. Arrows represent inferred variation of pH during overlapping or oscillating jarosite–hematite mineralization.

The lesson from this study of terrestrial jarosite is that without samples from Mars in hand we can do little more than identify the jarosite occurrence on Mars and infer that we have a deposit that formed at low pH from K-rich brines under oxidizing conditions. We are not be able to use the Ar–Ar dating technique (or other radiogenic dating techniques) to establish the age of sulfate deposition, and we cannot measure the stable isotope ratios O, S, and H to gain information on temperatures of formation, environments of deposition, or sources of fluids. In situ methods (for example, XRD) are able to distinguish jarosite from natrojarosite. However, martian sample return of surface deposits is a long time away and in the mean time we continue to look for meteorites from Mars. Although martian meteorites are mainly basalts and cumulate lithologies, some low temperature alteration phases have been identified (McSween and Treiman, 1998). These phases include

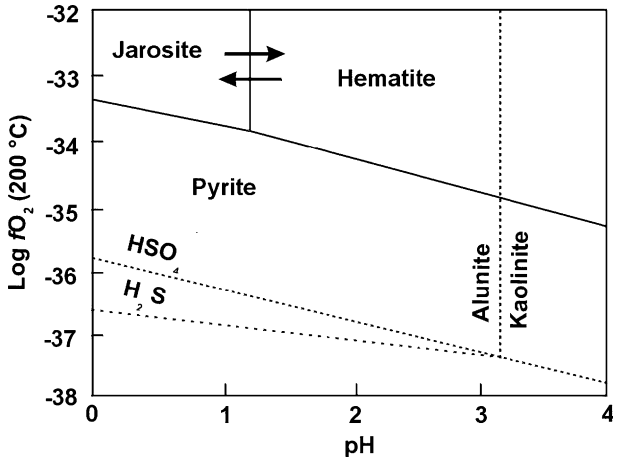

Fig. 10. Diagram showing jarosite stability on a diagram of LogfO_2 versus pH after Lueth et al. (2005). See that paper for assumptions concerning diagram construction.

sulfates and carbonates, and it is likely that eventually we will find martian meteorites that contain veins of sulfate assemblages that include jarosite. These will be truly valuable samples.

4.3. Case study: alunite and jarosite, Goldfield, Nevada

Keith et al. (1979) describe the occurrence of alunite and jarosite crystals in the epithermal precious-metal deposits of the Goldfield mining district, Nevada (Fig. 11). The district is part of a Tertiary volcanic center in which the rocks range from andesite to rhyolite. The sample described is from Preble Mountain, in the southern part of the area. The jarosite yielded a K–Ar age of 20 million years that is concordant with the age of mineralization. The normal sequence of crystallization is alunite followed by jarosite (Fig. 11). Initially, alunite formed comb-like growths

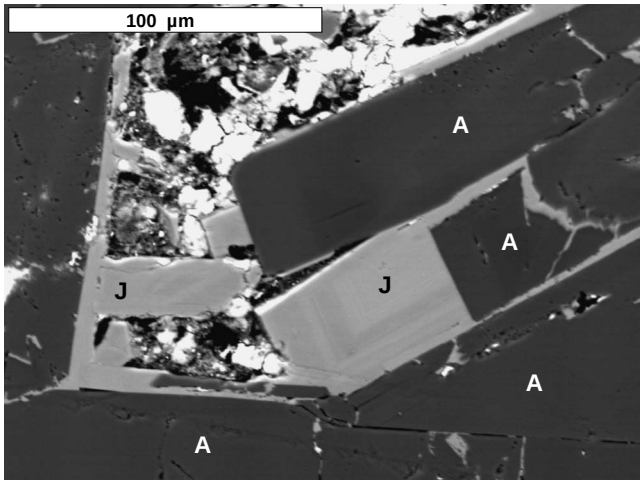

Fig. 11. BSE image of alunite (A) and jarosite (J) crystals from Goldfield, Nevada. Note the occurrence of jarosite crystals filling in vugs, open spaces, and fractures among alunite crystals; suggesting jarosite crystallization follows alunite crystallization.

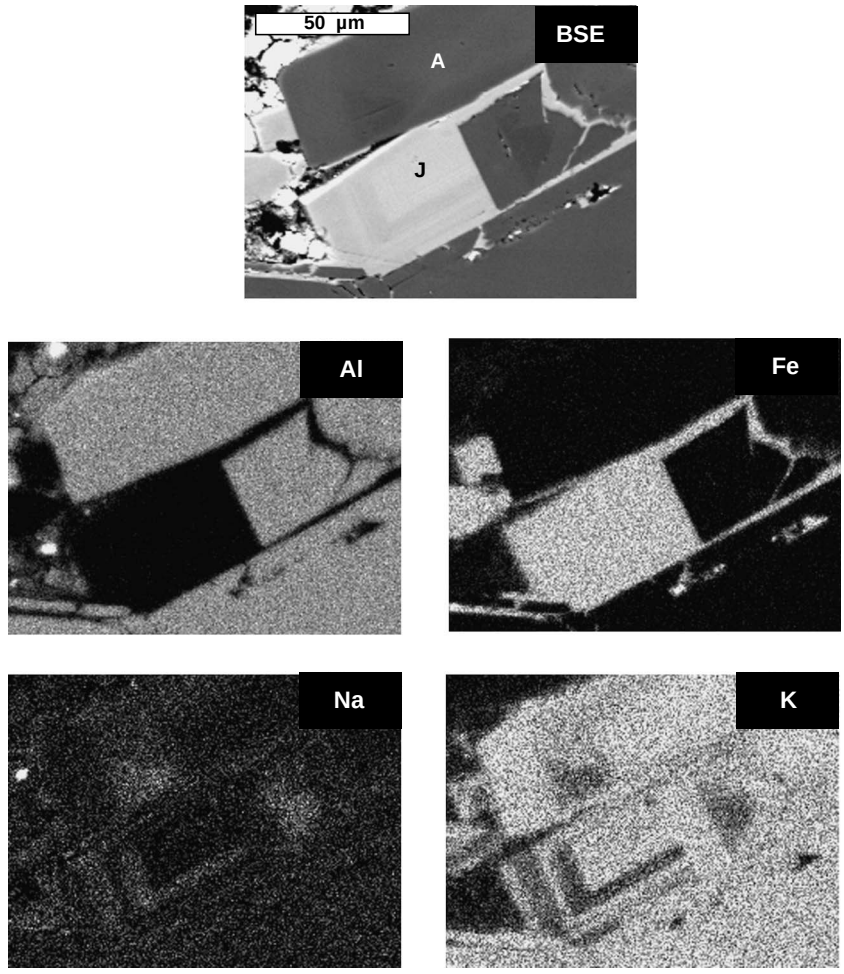

Fig. 12. Magnified BSE image of Fig. 11 and corresponding X-ray maps of the coexisting alunite (A) and jarosite (J). See text for discussion.

surrounding silicified rock breccia fragments that extend into fractures and vugs. Then both alunite and jarosite formed crystalline aggregates lining the vugs. In the final stage, jarosite alone crystallized and encrusted the remaining vein walls. Where the aggregates were absent, jarosite filled open spaces among alunite crystals and formed terminations on some. Fig. 12 shows alunite and jarosite and the accompanying X-ray maps illustrate their distinct compositions with respect to Al and Fe. The X-ray maps also show oscillatory zoning with respect to Na and K in the jarosite crystal. Keith et al. (1979) state that the two minerals formed in one of two ways: (1) all of the Preble Mountain localities were first deficient in iron and then were flooded with iron-rich solutions, or (2) the late-stage hydrothermal fluids underwent a change in Eh and pH, thus oxidizing existing Fe^{2+} in solution to Fe^{3+} and thus precipitating jarosite. The latter scenario is illustrated in Fig. 13, while evidence for the late stage precipitation of jarosite on alunite growth surfaces and fracture fillings is shown in Fig. 11. The late-stage precipitation of jarosite also shows oscillatory zoning, which reflects the Na/K evolution of the fluid. We intend to analyze the Goldfield samples for

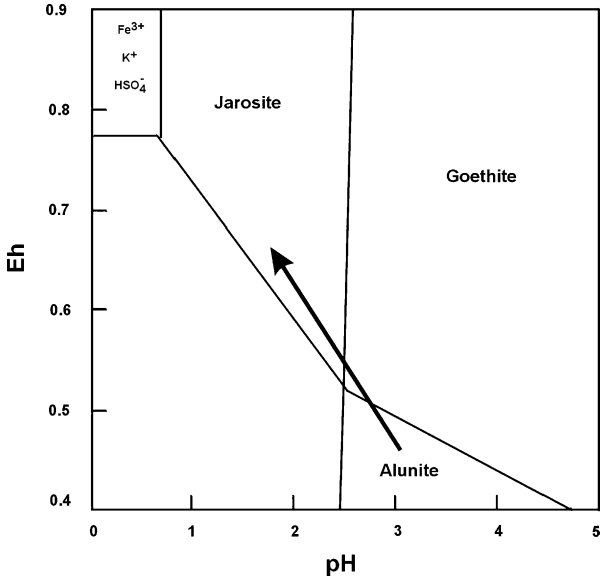

Fig. 13. Eh-pH diagram showing possible fluid evolution trajectory to produce coexisting alunite and jarosite crystals from Goldfield, Nevada. Diagram after Keith et al. (1979). See that paper for assumptions in constructing the diagram. See text for discussion.

numerous major, minor, and trace elements by both EMP and SIMS traverses across both alunite and jarosite crystals. We hope this study will give us additional important insights concerning fluid evolution.

Once again, a lesson for Mars exploration is that we need the samples to do these kind of studies. No in situ instruments are up to the task.

4.4. Case study: equilibrium mineral-fluid calculations and application to solid solution between alunite and natroalunite, El Indio-Pascua Belt, Chile and Argentina

Deyell and Dipple (2005) studied the effects of temperature and bulk fluid K/Na on the alunite–natroalunite solid solution at 200 bars and 100–300 °C. The authors claim that these are the conditions typical of magmatic–hydrothermal alteration and precious-metal mineral deposition in high-sulfidation environments that are characterized by the presence of alunite-bearing alteration zones. Their model is based on published experimental parameters that indicate both alunite and natroalunite are stable over this temperature range and that increased Na substitution is favored at higher temperatures. The modeling results indicate that a large variation in fluid K/Na is required to precipitate both K- and Na-alunite at high temperature. At lower temperature, much less variation in fluid composition can yield compositions near those of end-members. Controls on alunite–natroalunite solid solution in natural systems were evaluated using electron-microprobe data on alunite–natroalunite solid solutions from gold deposits of the El Indio-Pascua belt. The results indicate that higher temperatures of deposition correlate with a greater range of Na substitution in alunite. Elevated Na content in alunite is also attributed to higher concentrations of Na in the source fluids.

Fig. 14 illustrates the Deyell and Dipple (2005) model. On the diagram bulk fluid K/Na is plotted versus temperature for compositions of mole fraction K (K/K + Na-atomic) in alunite from 0.1 to 0.9. The solid line represents the position of the solvus between Na-alunite solid solutions and K-alunite solid solutions. The diagram shows that significant changes in equilibrium-fluid K/Na occur with increasing temperature at each solid solution composition.

This research indicates that estimates of the fluid K/Na ratio can be made if we can determine the K/Na ratio of the alunite and we can make an independent estimate of the temperature of deposition. Fig. 15 (schematic diagram after Alpers et al., 1992) illustrates the variation of the alunite and jarosite unit cell parameters with Na–K substitutions. Thus for terrestrial samples we have a variety of ways of exploiting this diagram (temperatures from fluid inclusion filling temperatures, EMP analyses, etc.). However, for martian samples, in situ measurements by XRD (see discussion below) can provide unit cell parameters that can indicate the K/Na ratio of alunite or jarosite but we would still need depositional temperature estimates to apply the diagram in Fig. 14.

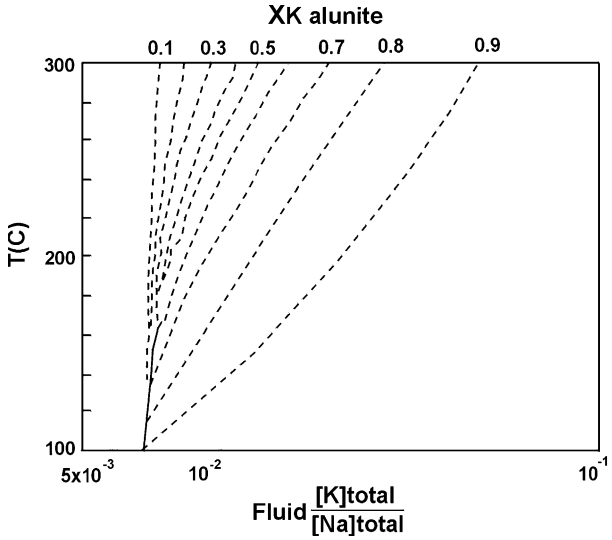

Fig. 14. Equilibrium compositions of alunite–natroalunite solid solution and coexisting fluid K/Na as a function of temperature. Solid line indicates calculated solvus between alunite and natroalunite at low temperature. Diagram after Deyell and Dipple (2005). See text for discussion.

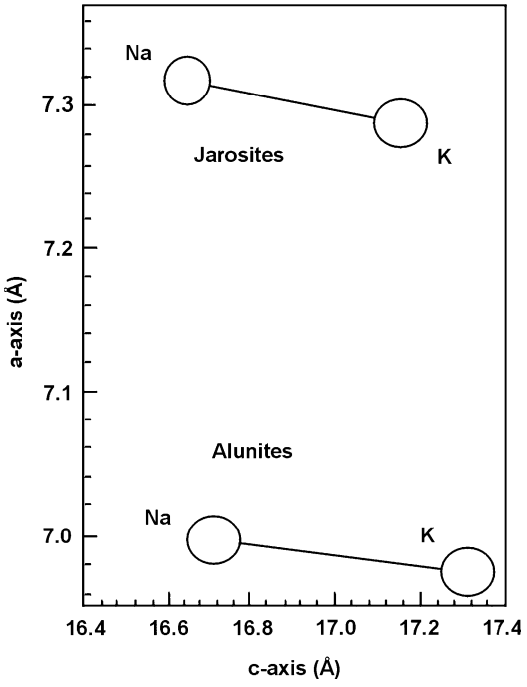

Fig. 15. Simplified diagram showing variation of *a*-axis and *c*-axis unit cell dimensions of alunite–natroalunite and jarosite–natrojarosite solid solutions after Alpers et al. (1992). See text for discussion.

4.5. Landed (in situ) XRD/XRF analysis by CheMin on Mars

Vaniman et al. (1998) describe CheMin, a miniaturized XRD/XRF instrument designed for space missions. This instrument has been selected for flight on the Mars Science Laboratory (MSL), with possible flights in 2009 and 2011. The instrument uses a transmission geometry, CCD detec-

tor, and CoKα radiation for sample analysis. The CCD is operated in single-photon counting mode to discriminate fluoresced X-rays for chemical analysis, and it detects the diffracted positions of primary X-rays for diffraction analysis. The ability to accumulate and integrate the entire circumference of each Debye diffraction ring, combined with a piezoelectric powder movement system, compensates for poor powder preparations that might be produced by a robotic sampling system. Using Rietveld analysis of the XRD results, robust identification of mineral phases, refinement of unit cell parameters, and other crystal structure information are attainable. Since preferred orientation effects are removed by grain movement in piezoelectric-driven sample mounts, mineral abundances can be obtained from full-pattern Rietveld analysis. Also, the combination of XRD and XRF data permits the calculation of mixing models from end member mineral compositions; for jarosite this approach may be particularly powerful in determining the A-site cation type (Fig. 15). Thus, the CheMin in situ instrument will enable more quantitative appraisal of martian mineralogy but we still must await sample return to use the full power of our terrestrial laboratories in order to unlock all the information contained in these martian rocks.

5. Conclusions

The identification of jarosite at the martian Meridiani Planum site by the Mössbauer instrument on the MER has profound implications for the conditions of surficial fluid/rock interactions on Mars. Terrestrial comparisons provide some insights into the importance of jarosite and the possible composition of brines on Mars.

Terrestrial studies of jarosite show that it forms in highly acidic (low pH), K-bearing brines under oxidizing conditions. A likely scenario for jarosite formation on Mars is that sulfur gases are released in shallow magmas largely as SO_2. The SO_2 then reacts with water in shallow aquifers or at the martian surface and forms H_2SO_4 and H_2S in solutions that already contain Fe^{2+}. In this reaction S^{4+} in SO_2 is both oxidized to S^{6+} and reduced to S^{2-}. This reaction is capable of oxidizing some Fe^{2+} to Fe^{3+}. However, H_2S must also be oxidized to provide the low pH required for jarosite stability. We suggest that the reduction of martian atmospheric CO_2 to CO can provide the oxidant needed in the absence of abundant free atmospheric oxygen as on Earth.

The crystal structure of jarosite–alunite is remarkable in its ability to accommodate many elements in the periodic table. This is because the three cation sites are very compliant and can accommodate a wide variety of elements with different sizes and charges. Jarosite is a robust chronometer on Earth for Ar–Ar and K–Ar techniques, and we believe that the U–Pb, Rb–Sr, and Nd–Sm systems will work well for martian sulfate deposits that have coexisting jarosite, gypsum, and/or anhydrite. These isotopic systematics will provide insights into martian crustal evolution and the timing and nature of fluid-rock-atmospheric interactions.

Several terrestrial case studies show that jarosite–alunite are powerful recorders of surficial chemical conditions, particularly when we can apply the full power of state of the art instrumentation available in terrestrial laboratories. The stable isotopes of O, H, and S provide a record of temperatures of formation, environments of deposition, fluids, and fluid/atmospheric interactions. If we could find and sample jarosite of a range of ages on Mars we would have a powerful recorder of martian atmospheric evolution.

Sample return from Mars is expensive and is a long time away. In the mean time, we should search martian meteorites for veins showing sulfur-rich brine alteration and the occurrence of jarosite.

Acknowledgments

This study was supported by a NASA/Cosmochemistry grant to J.J.P. We thank reviewers Virgil Lueth and John Hughes, whose comments greatly improved the paper. Associate editor Clive Neal is thanked for handling this manuscript in a very expeditious manner. Thanks to Roger Ashley, USGS, for providing the alunite–jarosite sample from Goldfield, NV. Special thanks go to Eric Dowty for providing the beautiful jarosite structure drawings.

Associate editor: Clive R. Neal

References

Alpers, C.N., Jambor, J.L., Nordstrom, D.K., 2000. Sulfate minerals—crystallography, geochemistry, and environmental significance. *Rev. Miner. Geochem.* **40**, 1–608.

Alpers, C.N., Rye, R.O., Nordstrom, D.K., White, L.D., King, B., 1992. Chemical, crystallographic and stable isotopic properties of alunite and jarosite from acid-hypersaline Australian lakes. *Chem. Geol.* **96**, 203–226.

Deyell, C.L., Dipple, G.M., 2005. Equilibrium mineral-fluid calculations and their application to the solid solution between alunite and natroalunite in the El Indio-Pascua belt of Chile and Argentina. *Chem. Geol.* **215**, 219–234.

Ebert, S.W., Rye, R.O., 1997. Secondary precious metal enrichment by steam-heated fluids in the Crofoot Lewis hot spring gold-silver deposit and relation to paleoclimate. *Econ. Geol.* **92**, 578–600.

Elwood Madden, M.E., Bodnar, R.J., Rimstidt, J.D., 2004. Jarosite as an indicator of water-limited chemical weathering on Mars. *Nature* **431**, 821–823.

Hurowitz, J.A., McLennan, S.M., Lindsley, D.H., Schoonen, M.A.A., 2005. Experimental epithermal alteration of synthetic Los Angeles meteorite: implications for the origin of martian soils and identification of hydrothermal sites on Mars. *J. Geophys. Res.* **110**, E07002.

Kargel, J.S., 2004. Proof for water, hints of life? *Science* **306**, 1689–1691.

Keith, W.J., Calk, L., Ashley, R.P., 1979. Crystals of coexisting alunite and jarosite, Goldfield, Nevada. *Shorter Contrib. Miner. Petr.* **1124-C**, C1–C5, Geological Survey Professional Paper.

Klingelhöfer, G., Morris, R.V., et al., 2004. Jarosite and hematite at Meridiani Planum from Opportunity's Mössbauer spectrometer. *Science* **306**, 1740–1745.

Lueth, V.W., Rye, R.O., Peters, L., 2005. "Sour gas" hydrothermal jarosite: ancient to modern acid-sulfate mineralization in the southern Rio Grande Rift. *Chem. Geol.* **215**, 339–360.

McLennan, S.M., Bell, J.F., III, et al., 2005. Provenance and diagenesis of impure evapororitic sedimentary rocks on Meridiani Planum, Mars. In

Lunar and Planetary Science XXXVI, Abstract #1884, Lunar and planetary Institute, Houston.

McSween Jr., H.Y., Treiman, A.H., 1998. Martian meteorites. *Rev. Miner.* **36**, 6-1–6-53.

Menchetti, S., Sabelli, C., 1976. Crystal chemistry of the alunite series: crystal structure refinement of alunite and synthetic jarosite. *N. Jahrb. Miner. Monatsh. H.* **9**, 406–417.

Okada, K., Hirabayashi, J., Ossaka, J., 1982. Crystal structure of natroalunite and crystal chemistry of the alunite group. *N. Jahrb. Miner. Monatsh. H.* **12**, 534–540.

Papike, J.J., Karner, J.M., Shearer, C.K., 2005. Comparative planetary mineralogy: valence state partitioning of Cr, Fe, Ti, and V among crystallographic sites in olivine, pyroxene, and spinel from planetary basalts. *Am. Miner.* **90**, 277–290.

Rye, R.O., 2005. A review of stable-isotope geochemistry of sulfate minerals in selected igneous environments and related hydrothermal systems. *Chem. Geol.* **215**, 5–36.

Rye, R.O., Stoffregen, R.E., 1995. Jarosite-water oxygen and hydrogen isotope fractionations: preliminary experimental data. *Econ. Geol.* **90**, 2336–2342.

Rye, R.O., Alpers, C.N., 1997. The stable isotope geochemistry of jarosite. *U.S. Geol. Surv. Open-File*, 88–97.

Sarrazin, P., Blake, D., Bish, D., Vaniman, D., Chipera, S., Collins, S.A., Elliot, S.T., 2000. In situ investigation of ices and hydrous minerals at the lunar poles using a combined X-ray fluorescence and diffraction instrument. *J. Phys. IV France* **10**, 343–352.

Scott, K.M., 1987. Solid solution in, and classification of, gossan-derived members of the alunite-jarosite family, northwest Queensland, Australia. *Am. Miner.* **72**, 178–187.

Shearer, C.K., Layne, G.D., Papike, J.J., Spilde, M.N., 1996. Sulfur isotope systematics in alteration assemblages in martian meteorite Allan Hills 84001. *Geochim. Cosmochim. Acta* **60**, 2921–2926.

Stoffregen, R.E., Alpers, C.N., Jambor, J.L., 2000. Alunite-jarosite crystallography, thermodynamics, and geochronology. *Rev. Miner. Geochem.* **40**, 453–479.

Vaniman, D., Bish, D., Blake, D., Elliott, S.T., Sarrazin, P., Collins, S.A., Chipera, S., 1998. Landed XRD/XRF analysis of prime targets in the search for past or present Martian life. *J. Geophys. Res.* **103**, 477-31,489.

Zimbelman, D.R., Rye, R.O., Breit, G., 2005. Origin of secondary sulfate minerals in active andesitic stratovolcanoes. *Chem. Geol.* **215**, 37–60.